Desalination and Water Treatment
www.deswater.com
doi: 10.5004/dwt.2019.23848

149 (2019) 31–42
May

Prediction and correction of scaling effects on velocity profile in hydraulic laboratory experiments

Lin Zhang[a,b,*], Yigang Wang[a,b], Dake Chen[a,b], Cheng Chen[c]

[a]*Key Laboratory of Coastal Disaster and Defence, Ministry of Education, Hohai University, Nanjing 210098, China, email: dr.linzhang.hhu@gmail.com (L. Zhang)*
[b]*College of Harbor, Coastal and Offshore Engineering, Hohai University, Nanjing 210098, China*
[c]*College of Civil Engineering, Fuzhou University, Fuzhou 350116, China*

Received 22 October 2018; Accepted 15 January 2019

ABSTRACT

Due to the geometric distortion in distorted hydraulic laboratory experiments, velocity profile cannot maintain as constant as required by the traditional criteria. Scaling effects, which lack quantitative researches, cannot be avoided even if the Froude and drag coefficient similitude criteria were satisfied. Prediction formulas of scaling effect rate are established in this research to theoretically reveal the quantitative relations between velocity profile distortion and experimental parameters. They are directly related to three parameters, distorted ratio, relative water depth, and relative bed roughness. In vertical direction, most effects happen near the bed and the deviation increases with distortion ratio. The similarity of secondary flow is worse and more complicated than that of stream-wise flow. The correction method, which is the improvement of traditional similitude criteria, can effectively reduce scaling effects when converting experimental results into their corresponding values in the prototype. Three dimensional numerical models are built to verify the accuracy of the prediction formulas and correction method.

Keywords: Distortion ratio; Laboratory experiments; Scaling effects; Correction method; 3-D numerical models

1. Introduction

Laboratory experiments are widely used in hydraulic researches dealing with fluvial, estuarine, and coastal engineering problems. Based on similitude criteria, features like topography, currents, sediments, and time are modeled in scales to investigate full-scale conditions that are difficult to create in the laboratory. There are two types of these models. The first one is normal model, whose geometric scales in both horizontal and vertical directions are the same. According to the similitude theory, it is regarded well similar with the prototype. But in most large-scale experiments where coast and space requirements are prohibitive, the water will be too shallow if normal models are chosen. In that case, the surface tension cannot be avoided, making the experiment impossible [1]. So the researchers have to build the other type, distorted models. To insure measurable depth and flow patterns, the depth should be enlarged. The vertical distribution will bring in scaling effects into the experiments.

The former researchers have done tons of work studying scaling effects. Scaling effects are inevitable, as long as the ratio of one parameter between model and prototype varies in either space or time; they found similarity unsatisfied in vertical distribution of velocity profile and the deviation increasing with distortion ratio [2–5]. Theoretically, distorted models cannot completely satisfy the similitude criteria, thus creating deviation in velocity profile and concentration profile. Geometric distorted models did underestimate the rate of energy dissipation and the aeration efficiency of prototype stepped spillways for similar flow conditions [6].

* Corresponding author.

Murzyn and Chanson quantitatively demonstrated that dynamic similarity of two-phase flows in hydraulic jumps cannot be achieved with a Froude similitude [7]. The research of Fischer and Holley stated that simple transposition of concentration profiles from model to prototype is not valid and models may magnify or reduce longitudinal dispersion [8]. Current methods used in scaling sediment transport result in a number of scale effects, decreasing the accuracy and applicability of scale models [9]. The kinematics of suspended sediment is inversely proportional to the distortion ratio of the physical model but proportional to the width-depth ratio and curvature ratio [10]. Dou conducted laboratory experiments of 5 different ratios, 2.5, 4, 6, 8.33, and 12.8, pointing out most effects on sediment transport at the bottom, especially when the distortion ratio is larger than 6 [11,12].

The method of numerical modelling in researches of scaling effects is first introduced by Liu and verified by establishing two series of numerical flume models [13]. Dou presented that selection of parameter values has great influence on modelling results and that numerical modelling can be a research method for scaling effects if the parameters were well selected [14]. Fang used three-dimensional (3-D) numerical simulation to prove that the discrepancy between the distorted model and the normal model in stream-wise velocity is acceptable, while the velocity shows differences in vertical and transverse directions [15]. After decades of development, there are mature theoretical foundation and computing methods for numerical modelling. In numerical models, the parameters like topographic conditions, boundary conditions, and distortion ratios, which are difficult to adjust in the laboratory, can be easily input into calculation. It increases the research efficiency. Since it is too difficult to build models of different distortion ratios in laboratory, numerical models can be used as substitutes.

Appropriate representation of flow is critical to modelling experiments focused on sediment transport, thermal diffusion, and so on, due to their sensibility to flow hydraulics [10,15]. Introduction of vertical distortion will lead to larger bottom slopes and hydraulic gradient, converting to errors in velocity distortion, and secondary current representation. Therefore, the distortion of velocity profile is important to be revealed. The current researches on scaling effects of distorted physical models are mostly based on semi-experiential theories and focus on qualitative results. The results differ because of the different quantities used in different researches, not yet coming to a full solution [16].

Quantitative relations between scaling effects and experimental parameters are urgently needed. Based on the vertical distribution of velocity profile and motion equations, this article will solve prediction formulas and propose corrections for a non-ideal flume for hydraulic research. 3-D numerical models of continuous distortion ratios are built to test the accuracy of the prediction formulas and the correction method.

2. Methodology

2.1. Traditional similitude criteria

Dynamic similarity requires geometric and kinematic similarity, as well as similar force polygons at relative locations in the prototype and model [17]. In traditional scaling modelling of flow, Newton's law requires that the ratios of all force vectors be equal.

Due to the dominance of gravity forces in flow with unpressured free surface, gravity similitude is applied in most scaled modelling experiments [17,18]. It is known as Froude similitude criterion for representing same scales of inertia force and gravity.

$$\lambda_{F_r} = \lambda_J^{1/2} \tag{1}$$

$$\lambda_u = \lambda_h^{1/2} \tag{2}$$

In addition, another significant force which must not be neglected in open channels is drag force. A kinematic similitude criteria should also include drag coefficient similarity [19]. With the combination of Chézy formula $u = C\sqrt{RJ}$, the criterion is solved as [20],

$$\lambda_C = \left(\frac{\lambda_l}{\lambda_R}\right)^{1/2} \tag{3}$$

2.2. Fundamental improvements of similitude criteria

Based on 2-D flow in open channels, this section intends to get a concise analytical solution for improvements of similitude criteria. In the following derivation, those with the subscript p represent the subjects' values in the prototype, while those with the subscript m represent the subjects' values in the models.

In open channels except for water affected by the wall function, the velocity profile corresponds to the logarithmic distribution [21].

$$\frac{du}{dz} = \frac{u_*}{\kappa z} \tag{4}$$

$$u = \frac{u_*}{\kappa}\ln\frac{z}{z_0} = \frac{u_*}{\kappa}\ln\frac{\eta}{\eta_0} \tag{5}$$

where $z_0 \infty \kappa_s$, $\eta_0 = z_0/D$ is a un-dimensional parameter related to κ_s/D.

The vertical distribution of velocity is related to depth and cannot maintain similarity in distorted models [3]. The velocity profile is absolutely distorted. The velocity at $0.6D$ below the water surface approximates the depth-averaged velocity, which can be regarded similar in the distorted models [22]. To model a similar stream-wise flow, Froude similitude criterion should be applied to depth-average velocity, as well as drag coefficient similitude criterion. It can be considered as the velocity redistributing vertically.

$$\lambda_{\bar{u}} = \lambda_h^{1/2} \tag{6}$$

$$\bar{u} = \int_{\eta_0}^{1} u d\eta \int_{\eta_0}^{1} \frac{u_*}{\kappa}\ln\frac{\eta}{\eta_0} d\eta = \frac{\sqrt{gRJ}}{\kappa}\left(\eta_0 - 1 - \ln\eta_0\right) = \frac{\sqrt{gRJ}}{\kappa}\left(-1 - \ln\eta_0\right) \tag{7}$$

Based on Chézy formula, the depth-average velocity is

$$\bar{u} = C\sqrt{RJ} \tag{8}$$

Combining Eqs. (7) and (8), a new un-dimensional parameter is introduced as relative roughness,

$$a = -\left(1 + \ln \eta_0\right) = \frac{\kappa C}{\sqrt{g}} \tag{9}$$

$R = D$ in wide and shallow channels.

$$\lambda_R = \lambda_h \tag{10}$$

In consideration of scaling effects on velocity profile, $u_p = \lambda_u u_m$, where λ_u is not as invariable as Eq. (2). (Derivation process in Appendix A)

$$\lambda_u = \left[\frac{1-\varepsilon^{1/2}}{\varepsilon^{1/2} + a_p/\left(1+\ln\eta\right)} + 1\right]\lambda_h^{1/2} \tag{11}$$

The transverse circulation in bend channel is studied for scaling effects on secondary circulation. Hydraulic factors are shown in Fig. 1. The stream-wise velocity profile is logarithmic as Rosovsky pattern [23]. The transverse velocity profile is calculated as [24],

$$\frac{u_\theta}{\bar{u}_\theta} = 1 + \frac{\sqrt{g}}{\kappa C}\left(1+\ln\eta\right) \tag{12}$$

$$u_r = \frac{D\bar{u}_\theta}{\kappa^2 r}\left[-\left(1.5\eta\ln\eta - 3.3\eta + 2.025\right) - \frac{\sqrt{g}}{\kappa C}\left(0.75\eta\ln^2\eta - 2.4\eta\ln\eta + 2\ln\eta + 2.4\eta\right) + \frac{2g}{\kappa^2 C^2}\left(1+\ln\eta\right)\right] \tag{13}$$

Improved similitude criteria for stream-wise and span-wise velocity profile are solved as (Derivation process in Appendix B)

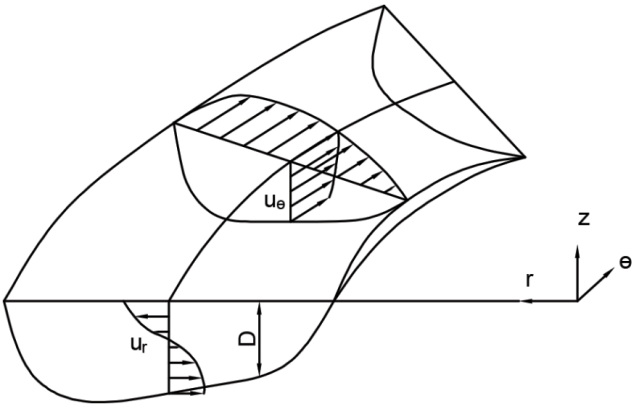

Fig. 1. Hydraulic factors in bend channels.

$$\lambda_{u_\theta} = \left[\frac{1-\varepsilon^{1/2}}{\varepsilon^{1/2} + a_p/\left(1+\ln\eta\right)} + 1\right]\lambda_h^{1/2} \tag{14}$$

$$\lambda_{u_r} = \frac{\lambda_h^{1/2}}{A\varepsilon^2 + B\varepsilon + E} \tag{15}$$

where the derivation process is in Appendix B and reference values of *A*, *B*, and *E* are listed in Table A1.

Eq. (14) is same as Eq. (11), again proving the accuracy of usage of logarithmic velocity profile.

Eqs. (14) and (15) are the improved similitude criteria of velocity profile in stream-wise flow and secondary flow. They can also be used as correction method of similitude criterion in Eq. (2) when converting modelling results into their corresponding values in the prototype. In this way, the scaling effects on velocity profile can be reduced, and the results will more resemble those in reality.

2.3. Prediction of scaling effects

$\Delta = (\lambda_u - \lambda_h^{1/2})/\lambda_h^{1/2}$ is introduced as scaling effect rate, which is the percentage of difference between the calculated value and the traditional similitude criterion among the traditional value.

For the stream-wise flow

$$\Delta = \frac{1-\varepsilon^{1/2}}{\varepsilon^{1/2} + a_p/\left(1+\ln\eta\right)} \tag{16}$$

For the secondary circulation

$$\Delta = \frac{1}{A\varepsilon^2 + B\varepsilon + E} - 1 \tag{17}$$

Eqs. (16) and (17) are prediction formulas, which can predict the scaling effects on velocity distortion when designing the experiment plan before performing it. The results are error rates for different locations in the vertical direction. According to the testing location concerned in the experiment, a distortion ratio whose effect within error-tolerant rate can be selected.

Eqs. (16) and (17) contain distortion ratio ε, but not λ_h nor λ_l. In a sense, scaling effect is the influence of distortion ratio on experimental results. The scaling effects on flow is directly linked with three parameters, the distortion ratio ε, the relative water depth η, and bed roughness which is reflected as $a = -1 - \ln\eta_0$ in the formulas. $\Delta = 0$, when $\varepsilon = 1$, which means that the velocity distribution cannot be affected by the distortion ratio only if it was in a normal model.

According to the formulas, the distortion of velocity profile is drawn in Fig. 2.

In Eq. (16),

$$\frac{\partial\Delta}{\partial\eta} = \frac{1-\varepsilon^{1/2}}{\eta\left[\varepsilon^{1/2}\left(1+\ln\eta\right) + a_p\right]^2} < 0 \tag{18}$$

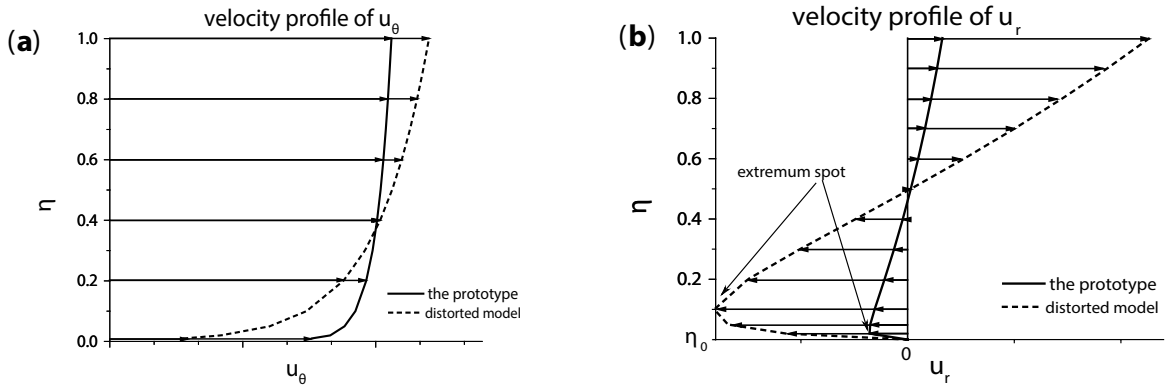

Fig. 2. Distortion of velocity profile of (a) the stream-wise flow and (b) the transverse circulation.

$$\frac{\partial \Delta}{\partial \varepsilon} = -\varepsilon^{1/2} \frac{a_p / (1+\ln\eta)+1}{2\left[\varepsilon^{1/2} + a_p/(1+\ln\eta)\right]^2} \quad \begin{cases} >0, & \eta < 0.37 (\Delta > 0) \\ <0, & \eta > 0.37 (\Delta < 0) \end{cases} \tag{19}$$

Δ is a decreasing function of η, that is, scaling effects decrease from bed to water surface and most effects happen near the bed. When η < 0.37, Δ > 0 and increases with the distortion ratio ε, that is, velocities in distorted models are faster than those in the prototypes. When η > 0.37, Δ < 0 and decreases with ε, which means velocities in distorted models are slower and the difference will be greater when ε increases. The distortion pattern is demonstrated in Fig. 2(a). The farther it is from 0.37*D*, the more distortion will be there. The velocity gets faster upon 0.37*D* while getting slower beneath it.

What Eq. (19) explains is that Δ moves away from 0 with ε increasing. So scaling effects on the stream-wise velocity profile would increase with distortion ratio.

In Eq. (17),

Assume $\frac{\partial u_r}{\partial \eta} = 0$, we can get the approximate solution of extremum value

$$u_{r\max}\Big|_{\eta=0.6a^{-1.285}} = \frac{u_\theta D}{\kappa^2 r}\left(-0.562\ln a + 0.1448\right) \tag{20}$$

The distortion makes the transverse circulation faster than it should be, which is quite similar with the distortion pattern of the stream-wise velocity. Displayed in Fig. 2(b), the transverse circulation rapidly increases to the extremum value from bed to the extreme spot $\eta = 0.6a^{-1.285}$. It reaches the maximum velocity toward the convex bank and then does not turn to the concave bank until it slightly reduces to zero. As given in Eq. (20), the extremum spot will move upward and its value will be enlarged in distorted models, causing the velocity profile more distorted around the extremum spot. Scaling effects on the transverse circulation velocity profile would also increase with distortion ratio.

Eqs. (15) and (17), which are based on transverse circulation, do not have any size information of bend channels. They could be used for secondary flow in other forms.

3. Validation and analysis

3.1. 3-D numerical modelling techniques

The numerical model solves the Reynolds averaged momentum equation by introduction of the hydrostatic assumption and the topography following sigma coordinate transformation, as well as the *k*-ε turbulent model, which has been widely applied in the channel computation [25]. The application of numerical technique is based on the finite volume method with unstructured grids. The wall boundary condition is zero normal velocity. Boundary conditions for numerical modelling include roughness height as bed roughness coefficient (Eq. (21)), as well as logarithmic velocity profile in turbulent boundary layers.

$$\frac{1}{n} = \frac{25.4}{\kappa_s^{1/6}} \tag{21}$$

To verify the deviated formulas, two series of 3-D numerical models with different distortion ratios are established. Model designing should follow the similitude criteria Eqs. (3)–(6). The values of designed parameters are listed in Table 1. To ignore the boundary effects, the width-depth ratio of each model is larger than 10 [26–32]. The depth is divided into 12 layers, as shown in Figs. 3 and 4. The modelling results will be used to test the accuracy of the prediction formulas in Eqs. (16) and (17) and verify the feasibility of the correction method in Eqs. (14) and (15).

3.2. Long open channels

Based on the designed parameters in Table 1, a series of long open channels are established as shown in Fig. 3. The channel length $L = 25B$.

In Fig. 5, comparisons of depth-average velocities along both $y = B/2$ and $y = B/4$ show high goodness of fit, except data near the entrance and exit. It means that the design of the models satisfies the similitude criteria. Displayed in Fig. 6, velocity is faster near the water surface and slower near the bed in distorted models, which coincides with the analysis of Eq. (11) [33–35]. Velocity gradient in distorted models is larger than that in the prototype and increases with distortion ratio. Especially, the tendency lines of prototype and

Table 1
Designed parameters in 3-D numerical modelling

Distortion ratio ε	Horizontal scale λ_l	Vertical scale λ_h	Channel width B(m)	Water depth h(m)	Average velocity $\bar{u}$(m/s)	Discharge Q(m^3/s)	Manning roughness n
Prototype	1	1	2,000	20	2	80,000	0.016
1	50	50	40	0.4	0.282843	4.525483	0.008336
2	200	100	10	0.2	0.2	0.4	0.010503
3	300	100	6.667	0.2	0.2	0.266667	0.012863
4	400	100	5	0.2	0.2	0.2	0.014853
5	500	100	4	0.2	0.2	0.16	0.016606
6	1,000	166.6667	2	0.12	0.154919	0.037181	0.016707
7	1,000	142.8571	2	0.14	0.167332	0.046853	0.018515
8	1,000	125	2	0.16	0.178885	0.057243	0.020239
9	1,000	111.1111	2	0.18	0.189737	0.068305	0.021892

($\varepsilon = \lambda_l/\lambda_h$, $\lambda_B = \lambda_l$, $\lambda_{\bar{u}} = \lambda_h^{1/2}$, $\lambda_Q = \lambda_h^{3/2}\lambda_l$, $\lambda_n = \lambda_R^{1/6}/\lambda_C = \lambda_h^{2/3}\lambda_l^{-1/2}$).

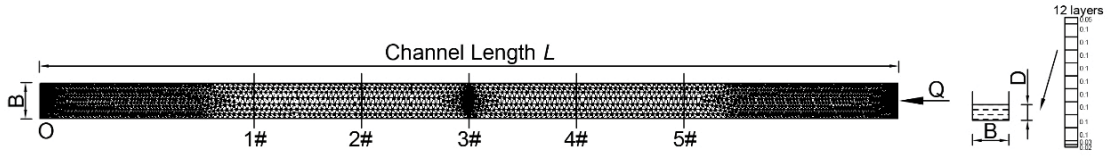

Fig. 3. 3-D numerical models in long open channel.

ε = 1 overlap, indicating that the geometric scales do not affect the numerical modelling.

In Fig. 7, predicted values of scaling effect rate are calculated by prediction Eq. (16), and calculated values are gained by applying numerical modelling results into $\Delta = (u_p/u_m - \lambda_h^{1/2})/\lambda_h^{1/2}$. The right Y-axis shows the corresponding relative depth η. As shown in Fig. 7, all the points gather around the correlation line $y = x$. It proves that the predicted values are consistent with the calculated values.

In each chart, the data of different positions overlap, indicating that the scaling effects are related only to relative roughness but independent of velocity or whole water depth, when the distortion ratio is settled [36–38]. So the formula can be applied not only to the individual locations but also to the whole water zone. In conclusion, Eq. (16) could be a good choice to estimate the scaling effects, as long as the experimental parameters are decided.

Characteristic patterns show among charts of Fig. 7, whose distortion ratios differ. In the layers of one location, Δ = 0 only when η = 0.37, that is, there is no scaling effect where the velocity equals the average velocity. Upon this, the velocity is faster due to distorted effects. But the error is not much, and the deviation value is usually within 15%. Underneath it, velocity is slower, and the influence should not be ignored. The closer the survey spot is to the bed, the lager the deviation, far exceeding 100%. In this example, most error is up to 300%, which happens in the model with a distortion ratio of 9. It is against experimental experiences but still meaningful. This is because that these data are extracted at η = 0.01, a position that most experiments cannot measure. The range of data set is wider when ε increases, showing more scaling effects on velocity distribution. It matches the regulation shown in Eq. (16), which is the deviation value nonlinear to distortion ratio. The distortion ratio and relative water depth are significant influence factors to the distortion of velocity profile.

3.3. Bend channels

The second series is of bend channels. The design of cross section is in accordance with Table 1. The bend angle is 180° to insure the transverse circulation well developed in the bends. The base slope along the channel is small while the lateral slope is 0. To reduce the boundary affection and guarantee turbulent evaluation, two strange channels, whose lengths are 5 times the radius of the bends R_b, are added as entrance and exit. Cross sections of angles 15°, 45°, 60°, 90°, 120°, 135°, and 165° are chosen as survey cross sections 1#, 2#, 3#, 4#, 5#, 6#, and 7#.

The centers of surveyed cross sections are chosen to verify the scaling effect rates of stream-wise velocity profile. According to Fig. 8, they are quite similar with those in long open channels. On account of its little value compared with stream-wise flow, the transverse circulation can hardly affect the stream-wise flow.

Since the scaling effect rates are identical with Eq. (16), this paper chooses one cross section, 1#, to display the correction method for stream-wise velocity. When converting the modelling results into their values in the prototype, the traditional similitude criterion Eq. (2) is used before correction, while improved criterion Eq. (14) is used after correction. As shown in Fig. 9, the correction method successfully reduces the scaling effects by making velocity profile closer to the prototype.

Cross sections 1#, 2#, 4#, and 6# are chosen to verify the correcting method of transverse velocity. When converting

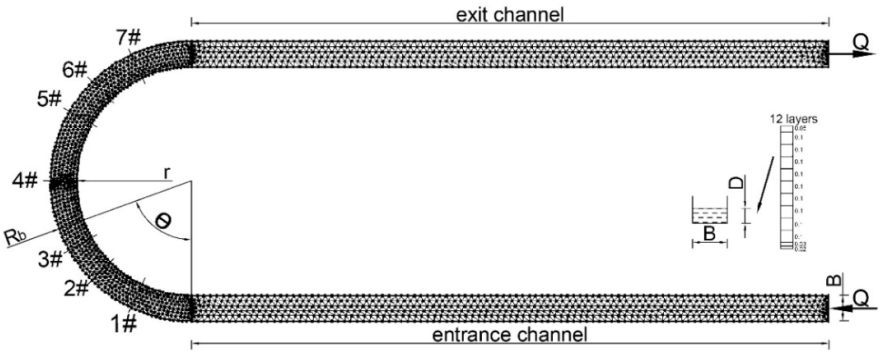

Fig. 4. 3-D numerical model in bend channels.

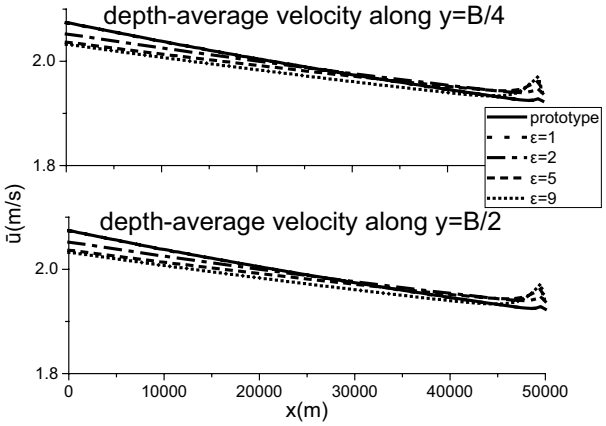

Fig. 5. Depth-average stream-wise velocity comparison.

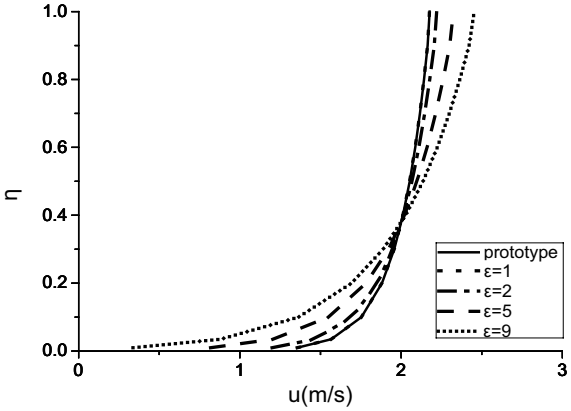

Fig. 6. Velocity profile at *L*/2, *B*/2.

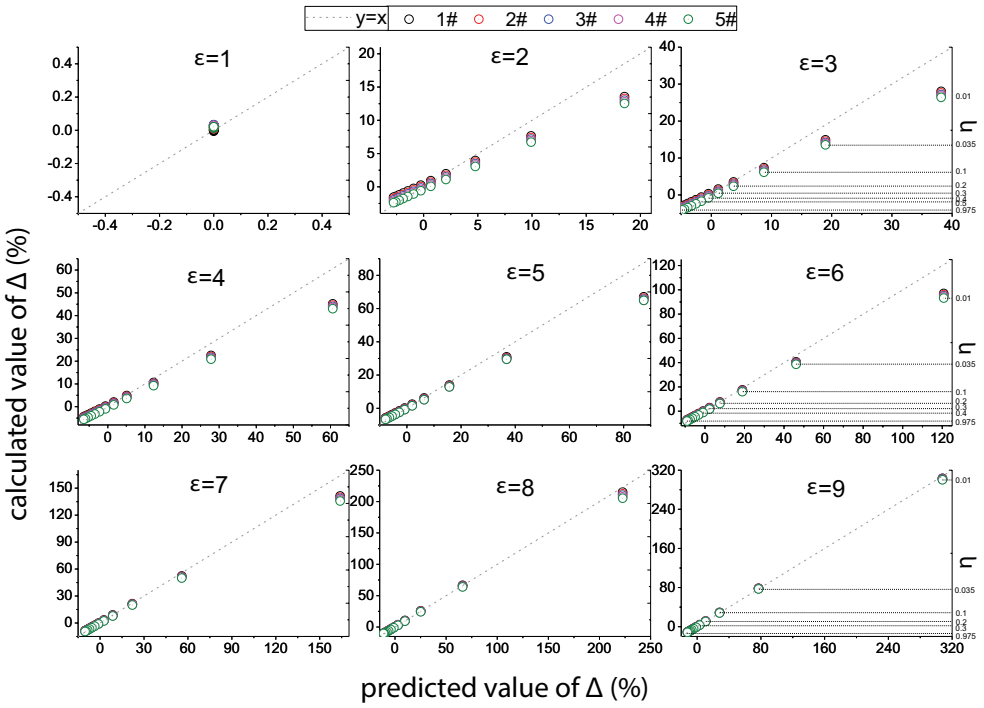

Fig. 7. Comparison of scaling effects between predicted and calculated values of stream-wise velocity profile in long open channels: predicted values of scaling effect rate are calculated by Eq. (16); calculated values are calculated by $\Delta = (u_p/u_m - \lambda_h^{1/2})/\lambda_h^{1/2}$.

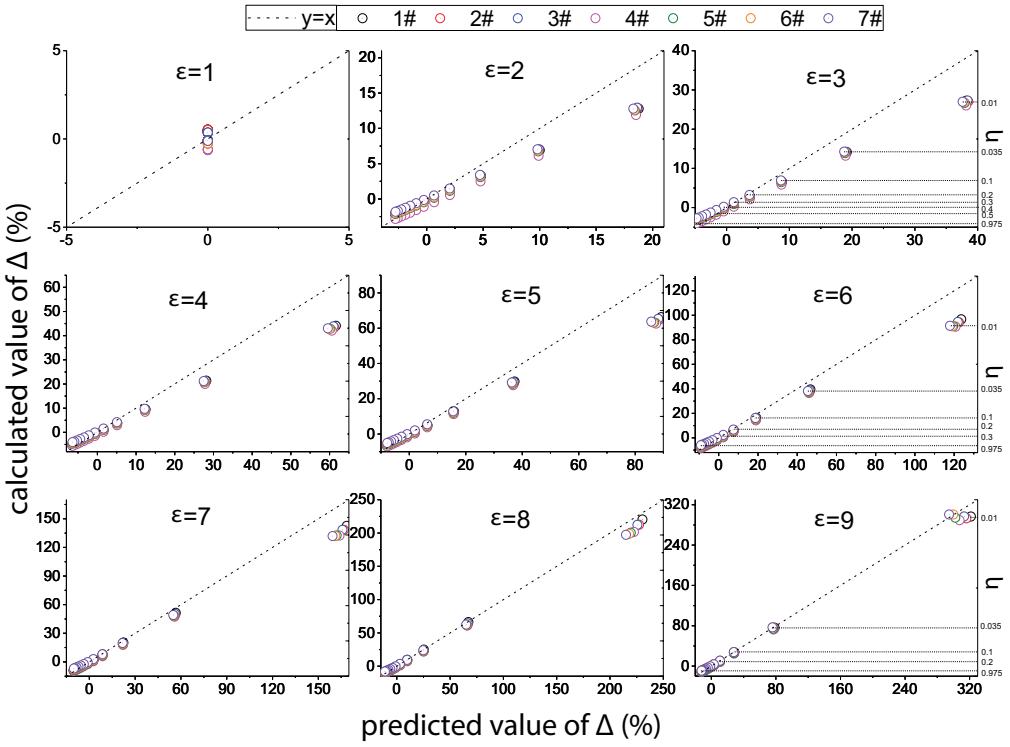

Fig. 8. Comparison of scaling effects between predicted and calculated values of stream-wise velocity profile in bend channels: predicted values of scaling effect rate are calculated by Eq. (16); calculated values are calculated by $\Delta = (u_p/u_m - \lambda_h^{1/2})/\lambda_h^{1/2}$.

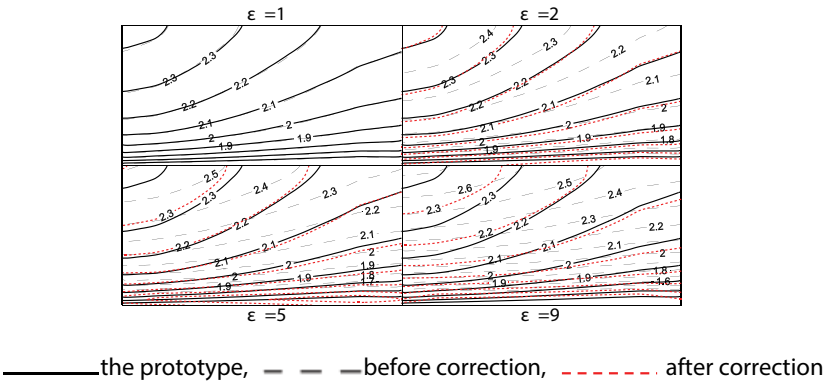

Fig. 9. The velocity profile of stream-wise velocity u_θ in bend channels before and after correction at cross section 1#, where Eq. (2) is used before correction and Eq. (14) is used after correction.

the modelling results into their values in the prototype, the traditional similitude criterion Eq. (2) is used before correction, while improved criterion Eq. (15) is used after correction.

Fig. 10 uses contour lines to show the distribution of transverse circulation u_r. The data before correction indicate that the scaling effects on transverse circulation is no longer numerical difference but a problem by orders of magnitude. At all the cross sections, the contour lines of ε = 1 are consistent with those of the prototype, even for cross section 1#, where the transverse circulation is still developing due to its short distance to the entrance. Deviation grows up from ε = 2 and rapidly increases with ε. Before correction, the contour lines of transverse circulation whose distortion ratios are 5 and 9 form observable circles near the bed. It is identical with the analysis that the extremum spot moves upward and is enlarged by times in distorted models.

The correcting method manages to eliminate the circles and reduces the enlargement, proving that the correction method for transverse circulation has enough accuracy. For all cross sections in ε = 2 and 5, the contour lines after correction move closer to the prototype. But the fitness is not so good for ε = 9, especially beside the banks. The transverse velocity is not fit with the values in prototype as well as ε = 1, but the deviation is successfully reduced by orders of magnitude.

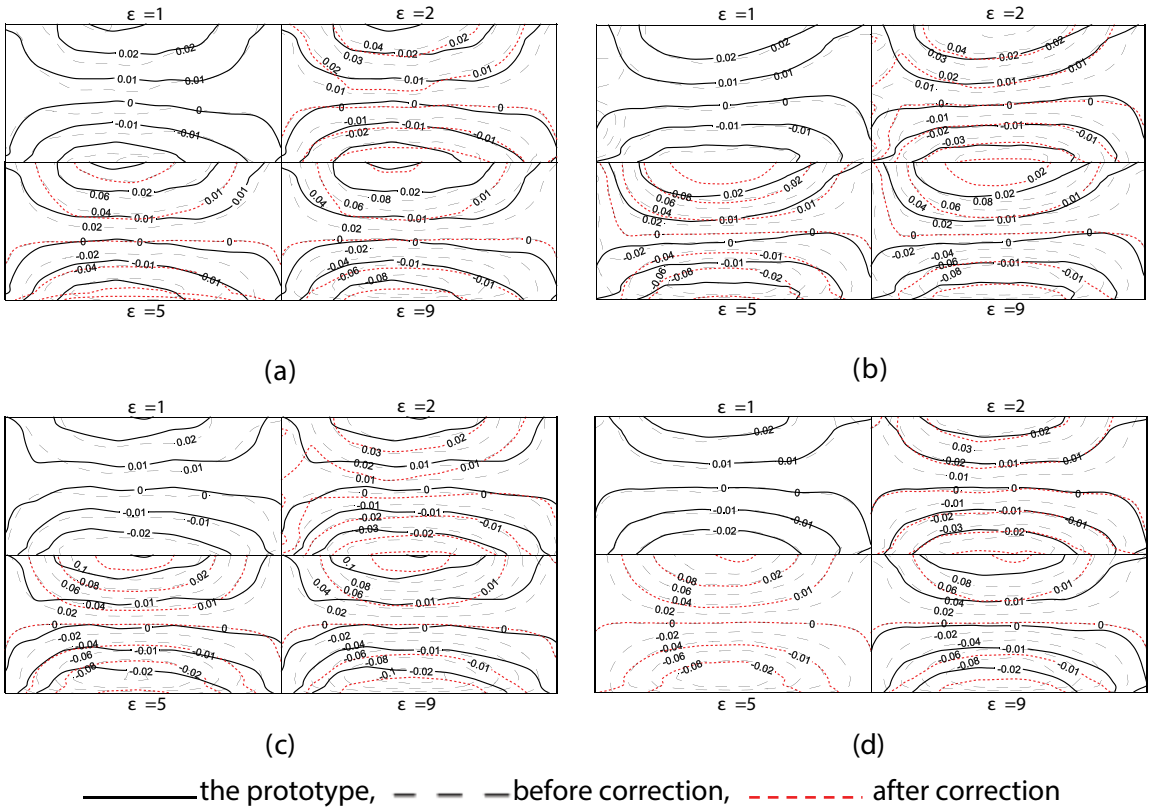

Fig. 10. The velocity profile of transverse circulation u_r in bend channels before and after correction: (a) at cross section 1#, (b) at cross section 2#, (c) at cross section 4#, and (d) at cross section 6#, where Eq. (2) is used before correction and Eq. (15) is used after correction.

Though the scaling effects are reduced by correction method, there are still discrepancies beside the channel banks. The more the model is distorted, the more the discrepancy. The reason is that the wall function cannot be covered by the mathematical derivation in Chapter 2. The turbulence near wall is strengthened in more distorted models, which is another scaling effect needed to be considered.

4. Conclusions

The scaling effects are no longer qualitative problems but can be calculated. By deriving mathematical formulas, scaling effects of different parameters are revealed in the prediction formulas of Eqs. (16) and (17). The introduction of the un-dimensional parameter, the relative roughness, helps to simplify the formula form, making the formulas more convenient to be applied.

On velocity profile, the effects are directly linked with distorted ratio, relative water depth, and relative bed roughness. For different experimental prototypes, the scaling effects will differ because of different parameters. The prediction formulas are appropriate for selecting a distortion plan within a certain tolerance.

The velocity gradients of both stream-wise velocity and transverse circulation are enlarged by geometric distortion, making a larger shear stress. It will surely affect the mass transport within the surveyed water.

The research finds the location where scaling effects affect most, which is in the bottom. Moreover, the effects increase when approaching the bed. According to this, when designing models focused on parameters close to bed, bedload transport for example, researchers must choose a distorted ratio as small as possible to avoid quadric errors.

The scaling effects are inevitable in distorted models but can be corrected by Eqs. (14) and (15), which are improvements for traditional criteria when converting experimental results into their corresponding values in the prototypes. There is still discrepancy but acceptable.

Numerical modelling can be applied to researches on scaling effects of distorted hydraulic laboratory experiments. The values of the parameters should be critically selected by the similitude criteria.

Symbols

a	—	Relative roughness, $a = -1 - \ln \eta_0$
C	—	Chézy coefficient, $C = R^{1/6}/n$
D	—	The whole water depth
ε	—	Distortion ratio, $\varepsilon = \lambda_l/\lambda_h$
F_r	—	Froude number, $F_r = \frac{u}{\sqrt{gl}}$
g	—	Gravity acceleration
h	—	Vertical height
J	—	Hydraulic gradient, $J = h/l$
K_s	—	Roughness height

l — Horizontal length
n — Roughness coefficient
P — The intensity of pressure
R — Hydraulic radius, $R = D$ in wide and shallow waters
u — Flow velocity
$\bar{u}$ — Depth-average velocity, $\bar{u} = \int_0^D u dz$
u_* — The friction velocity, $u_* = \sqrt{gRJ}$
z — The height to the bed
z_0 — the height where $u_x = u_y = 0$
η — The relative depth, $\eta = z/D$
κ — Von Karman coefficient
λ — Scale of its subscript, $\lambda_f = f_p/f_m$
λ_h — Vertical geometric scale
λ_l — Horizontal geometric scale
μ_t — Eddy viscosity coefficient
ν — Fluid kinematic viscosity
ρ — Fluid density

Subscripts

m — Value in the model
p — Value in the prototype
r — Span-wise coordinate axis
z — Vertical coordinate axis
θ — Stream-wise coordinate axis

Acknowledgement

The research is supported by *Basic Scientific Research Foundation of Central Universities, Jiangsu Province* (2015B35014).

References

[1] J.H. Xie, Simulation for Rivers, Water Conservancy and Electric Power Press, Beijing, 1990.
[2] M. De Vries, Application of Physical and Mathematical Models for River Problems, Delft Hydraulic Laboratory, ISRM, 1973.
[3] B. Lin, On the criterion of similarity of sediment diffusion in distorted models, Yangtze River, 25 (1994) 1–6.
[4] M. Qu, Similarity criteria and modelling techniques of movable-bed models for the yellow river, J. Sediment. Res., 3 (1981) 29–42.
[5] W. Li, Preliminary study on vertical velocity distribution of distorted river model, J. Waterw. Harbor, 22 (2001) 113–117.
[6] S. Felder, H. Chanson, Turbulence, dynamic similarity and scale effects in high-velocity free-surface flows above a stepped chute, Exp. Fluids, 47 (2009) 1–18.
[7] F. Murzyn, H. Chanson, Experimental assessment of scale effects affecting two-phase flow properties in hydraulic jumps, Exp. Fluids, 45 (2008) 513–521.
[8] H.B. Fischer, E.R. Holley, Analysis of the use of distorted hydraulic models for dispersion study, Water Resour. Res., 7 (1971) 46–51.
[9] K.J. Carr, A. Ercan, M.L. Kavvas, Scaling and self-similarity of one-dimensional unsteady suspended sediment transport with emphasis on unscaled sediment material properties, J. Hydraul. Eng., 141 (2015) 04015003.
[10] J. Lu, X. Liao, G. Zhao, Experimental study on effects of geometric distortion upon suspended sediments in bending channels, Sediment. Geol., 294 (2013) 27–36.
[11] X. Dou, F. Dong, Effect of distortion ratio on local scour under tidal currents and waves, China Ocean Eng., 18 (2004) 613–628.
[12] X. Dou, The Effects of Distortion Ratios on Tidal Currents, Waves and Sediment Models, Hohai University, 2005.
[13] J. Liu, H. Fang, R. Fu, Use of mathematical model to research scale rate of physical model, J. Hydrodyn., 20 (2005) 132–145.
[14] X. Dou, X. Zhang, H. Qu, Discussion about mathematical modelling applied to distortion ratios, COES, Nanjing, 2007, pp. 419–426.
[15] H. Fang, G. He, J. Liu, M. Chen, 3D numerical investigation of distorted scale in hydraulic physical model experiments, J. Coast. Res., 10052 (2008) 41–54.
[16] G. Ranieri, The surf zone distortion of beach profiles in small–scale coastal models, J. Hydraul. Res., 45 (2007) 261–269.
[17] R. Amdt, P. Roberts, T. Wahl, Hydraulic modeling: concepts and practice, ASCE Manuals and Reports on Engineering Practice, New York, 97 (2000) 390.
[18] W. Huang, Q. Yang, H. Xiao, CFD modeling of scale effects on turbulence flow and scour around bridge piers, Comput. Fluids, 38 (2009) 1050–1058.
[19] S. Gu, L. Ren, X. Wang, H. Xie, Y. Huang, J. Wei, S. Shao, SPHysics simulation of experimental spillway hydraulics, Water, 9 (2017) 973.
[20] C.Z. Chen, S.I. Zhang, J.M. Ma, Influence of distorted model on flow kinematic similitude, Water Resour. Hydropower Eng., 38 (2007) 35–38.
[21] G.H. Keulegan, Laws of turbulent flow in open channels, J. Res. Nat. Bur. Stand., 21 (1938) 707–741.
[22] G. Zhao, P.J. Visser, J. Lu, J.K. Vrijling, Similarity of the velocity profile in geometrically distorted flow model, Flow Meas. Instrum., 32 (2013) 107–110.
[23] И.Л. Rosovsky, X. Yin, Investigation of flow in bend channels, J. Sediment. Res., 1 (1958) 83–95.
[24] Z. Song, The universal formula on transverse circulation in channel bends, J. Sediment. Res., 4 (2003) 19–23.
[25] W. Dai, M. Ding, H. Zhang, On the difference of river resistance computation between the k–ε model and the mixing length model, Water, 10 (2018) 870.
[26] C. Li, D. Jin, Model Test of River Engineering, China Communication Press, Beijing, 1981, 252 p.
[27] Z. Liu, W. Peng, Y. Zare, D. Hui, K.Y. Rhee, Predicting the electrical conductivity in polymer carbon nanotube nanocomposites based on the volume fractions and resistances of the nanoparticle, interphase, and tunneling regions in conductive networks, RSC Adv., 8 (2018) 19001–19010.
[28] T.E. Bell, J.M. Gonzalez-Carballo, R.P. Tooze, L. Torrente-Murciano, High yield manufacturing of gamma-Al_2O_3 nanorods, ACS Sustainable Chem. Eng., 6 (2018) 88–92.
[29] W. Gao, L. Zhu, Y. Guo, K. Wang, Ontology learning algorithm for similarity measuring and ontology mapping using linear programming, J. Intell. Fuzzy Syst., 33 (2017) 3153–3163.
[30] H.H. Mohamed, N.A. Alomair, Exploiting stored TiO_2 Electrons for multi-electron reduction of an azo dye methyl orange in aqueous suspension, J. Saudi Chem. Soc., 22 (2018) 322–328.
[31] P. Szymak, Comparison of fuzzy system with neural aggregation FSNA with classical TSK fuzzy system in anti-collision Problem USV, Polish Marit. Res., 24 (2017) 3–14.
[32] W. Peng, S. Ge, A.G. Ebadi, H. Hisoriev, M.J. Esfahani, Syngas production by catalytic co-gasification of coal-biomass blends in a circulating fluidized bed gasifier, J. Cleaner Prod., 168 (2017) 1513–1517.
[33] M. Sudhakaran, D. Ramamoorthy, V. Savitha, S. Balamurugan, Assessment of trace elements and its influence on physico-chemical and biological properties in coastal agroecosystem soil, Puducherry region, Geol. Ecol. Landscapes, 2 (2018) 169–176.
[34] C. Emeh, O. Igwe, Effect of environmental pollution on susceptibility of sesquioxide-rich soils to water erosion, Geol. Ecol. Landscapes, 2 (2018) 115–126.
[35] H. Uddina, A.B.M. Alaamaa, I.S.M. Zaidul, S.A. Abbasb, M. Awang, T.K. Fahim, Current analytical methods for amlodipine and its formulations: a review, J. CleanWAS, 1 (2017) 17–22.

[36] K. Kudus, I. Grasian, S. Madasamy, A. John, Immunomodulatory effect of alginic acid from brown seaweed Sargassum wightii on disease resistance in Penaeus monodon, J. CleanWAS, 1 (2017) 26–29.
[37] M. Afzal, M.A. Rizwan, To assess the trends of living and poverty in a desert climate, Water Conserv. Manage., 1 (2017) 15–18.
[38] G. Yun, S. Williams, D. Wenbin, Water management of the Mekong River, Water Conserv. Manage., 1 (2017) 10–12.

Appendix A

$R = D$ in wide and shallow channels.

$$\lambda_R = \lambda_h \tag{A.1}$$

$$\lambda_C = \left(\frac{\lambda_l}{\lambda_R}\right)^{1/2} = \left(\frac{\lambda_l}{\lambda_h}\right)^{1/2} = \varepsilon^{1/2} \tag{A.2}$$

$$\lambda_a = \frac{1+\ln\eta_{0p}}{1+\ln\eta_{0m}} = \frac{\lambda_\kappa \lambda_C}{\lambda_g^{-1/2}} = \varepsilon^{1/2} \tag{A.3}$$

$$u_p = \frac{u_{*p}}{\kappa}\ln\frac{\eta_p}{\eta_{0p}} \tag{A.4}$$

$$u_m = \frac{u_{*m}}{\kappa}\ln\frac{\eta_m}{\eta_{0m}} \tag{A.5}$$

$$\lambda_u = \frac{u_p}{u_m} = \frac{u_{*p}}{u_{*m}} \times \frac{\ln\eta - \ln\eta_{0p}}{\ln\eta - \ln\eta_{0m}} = \varepsilon^{-1/2}\lambda_h^{1/2}\frac{1+\ln\eta-\left(1+\ln\eta_{0p}\right)}{1+\ln\eta-\left(1+\ln\eta_{0m}\right)} \tag{A.6}$$

$$\lambda_u = \left[\frac{1-\varepsilon^{1/2}}{\varepsilon^{1/2}+a_p/\left(1+\ln\eta\right)}+1\right]\lambda_h^{1/2} \tag{A.7}$$

Appendix B

The transverse velocity profile is calculated as

$$\frac{u_\theta}{\bar{u}_\theta} = 1 + \frac{\sqrt{g}}{\kappa C}\left(1+\ln\eta\right) \tag{B.1}$$

$$u_r = \frac{D\bar{u}_\theta}{\kappa^2 r}\left[-\left(1.5\eta\ln\eta - 3.3\eta + 2.025\right) - \frac{\sqrt{g}}{\kappa C}\left(0.75\eta\ln^2\eta - 2.4\eta\ln\eta + 2\ln\eta + 2.4\eta\right) + \frac{2g}{\kappa^2 C^2}\left(1+\ln\eta\right)\right] \tag{B.2}$$

Substitute $a = \kappa C/\sqrt{g}$ into Eq. (B.1) and Eq. (13), the velocity scales are calculated as

$$\frac{u_\theta}{\bar{u}_\theta} = 1 + \frac{\left(1+\ln\eta\right)}{a} \tag{B.3}$$

$$u_r = \frac{D\bar{u}_\theta}{\kappa^2 r}\left[-\left(1.5\eta\ln\eta - 3.3\eta + 2.025\right) + \frac{1}{a}\left(-0.75\eta\ln^2\eta + 2.4\eta\ln\eta - 2\ln\eta - 2.4\eta\right) + \frac{2}{a^2}\left(1+\ln\eta\right)\right] = \frac{\bar{u}_\theta D}{\kappa^2 r}F \tag{B.4}$$

where $F = F_0 + \frac{1}{a}F_1 + \frac{1}{a^2}F^2$, F_0 = 3.3η – 1.5η lnη – 2.025, F_1 = – 0.75η ln²η + 2.4η lnη – 2lnη – 2.4η, F_2 = 2(1 + lnη).

$$\frac{\lambda_{u_\theta}}{\lambda_{\bar{u}_\theta}} = \frac{1+\left(1+\ln\eta\right)/a_p}{1+\left(1+\ln\eta\right)/a_m} \tag{B.5}$$

$$\lambda_{u_\theta} = \lambda_h^{1/2}\frac{1+\left(1+\ln\eta\right)/a_p}{1+\left(1+\ln\eta\right)\varepsilon^{1/2}/a_p} \tag{B.6}$$

$$\lambda_{u_\theta} = \left[\frac{1-\varepsilon^{1/2}}{\varepsilon^{1/2}+a_p/\left(1+\ln\eta\right)}+1\right]\lambda_h^{1/2} \tag{B.7}$$

Eq. (14) is same with Eq. (A.7), again proving the accuracy of usage of logarithmic velocity profile.

$$\lambda_{u_r} = \lambda_{\bar{u}_\theta}\frac{F_p}{\varepsilon F_m} = \lambda_h^{1/2}\frac{F_p}{\varepsilon F_m} \tag{B.8}$$

To simplify Eq. (B.8), the approximate values are applied by least square method.

$$\frac{\varepsilon F_m}{F_p} = \varepsilon\frac{F_0}{F_p} + \frac{\varepsilon^{3/2}}{a_p}\times\frac{F_1}{F_p} + \frac{\varepsilon^2}{a_p^2}\times\frac{F_2}{F_p} = A\varepsilon^2 + B\varepsilon + E \tag{B.9}$$

where A, B, and E are undetermined parameters related to η and a_p.

$$S = \int_1^{10}\left[\left(\frac{F_2}{a_p^2 F_p} - A\right)\varepsilon^2 + \frac{F_1}{a_p F_p}\varepsilon^{3/2} + \left(\frac{F_0}{F_p} - B\right)\varepsilon - E\right]^2 d\varepsilon \tag{B.10}$$

$$\begin{cases} \dfrac{\partial S}{\partial A} = 39999.6A + 4999.5B + 666E - \left(39999.6 \times \dfrac{F_2}{a_p^2 F_p} + 14054.12 \times \dfrac{F_1}{a_p F_p} + 4999.5 \times \dfrac{F_0}{F_p} \right) = 0 \\ \dfrac{\partial S}{\partial B} = 4999.5A + 666B + 99E - \left(4999.5 \times \dfrac{F_2}{a_p^2 F_p} + 1806.44 \times \dfrac{F_1}{a_p F_p} + 666 \times \dfrac{F_0}{F_p} \right) = 0 \\ A + B + E = 1 \end{cases}$$

$$\Rightarrow \begin{cases} A = 0.048 + 0.95 \times \dfrac{F_2}{a_p^2 F_p} + 0.13 \times \dfrac{F_1}{a_p F_p} - 0.048 \times \dfrac{F_0}{F_p} \\ B = -0.59 + 0.59 \times \dfrac{F_2}{a_p^2 F_p} + 2.05 \times \dfrac{F_1}{a_p F_p} + 1.59 \times \dfrac{F_0}{F_p} \\ E = 1.54 - 1.54 \times \dfrac{F_2}{a_p^2 F_p} - 2.18 \times \dfrac{F_1}{a_p F_p} - 1.54 \times \dfrac{F_0}{F_p} \end{cases}$$

$$\lambda_{u_r} = \frac{\lambda_h^{1/2}}{A\varepsilon^2 + B\varepsilon + E} \tag{B.11}$$

Reference values of *A*, *B*, and *E* are listed in Table A1.

Table A1
Reference values of *A*, *B*, and *E*

a_p η\A	3	4	5	6	7	8	10	12	14	16	18	20
0.01	−1.09	0.368	−0.069	−0.101	−0.1	−0.093	−0.079	−0.067	−0.058	−0.051	−0.046	−0.041
0.05	0.385	0.032	−0.033	−0.048	−0.051	−0.05	−0.045	−0.04	−0.035	−0.032	−0.029	−0.026
0.1	0.173	0.016	−0.023	−0.034	−0.037	−0.037	−0.034	−0.03	−0.027	−0.024	−0.022	−0.02
0.2	0.086	0.011	−0.012	−0.02	−0.022	−0.023	−0.022	−0.02	−0.018	−0.016	−0.015	−0.014
0.3	0.044	0.009	−0.003	−0.008	−0.01	−0.01	−0.01	−0.01	−0.009	−0.008	−0.008	−0.007
0.4	−0.013	0.006	0.014	0.017	0.018	0.018	0.017	0.016	0.015	0.014	0.013	0.012
0.5	−0.298	−0.055	−1.155	−0.311	−0.217	−0.172	−0.125	−0.1	−0.083	−0.071	−0.062	−0.055
0.6	0.336	0.027	−0.032	−0.047	−0.05	−0.049	−0.044	−0.039	−0.034	−0.031	−0.028	−0.025
0.7	0.179	0.023	−0.018	−0.031	−0.034	−0.035	−0.032	−0.029	−0.026	−0.024	−0.021	−0.02
0.8	0.142	0.022	−0.012	−0.024	−0.028	−0.029	−0.027	−0.025	−0.022	−0.02	−0.019	−0.017
0.9	0.125	0.022	−0.009	−0.02	−0.024	−0.025	−0.024	−0.022	−0.02	−0.018	−0.017	−0.015
1	0.115	0.023	−0.007	−0.017	−0.021	−0.022	−0.022	−0.02	−0.018	−0.017	−0.015	−0.014
B												
0.01	9.735	−9.236	−1.592	−0.388	0.079	0.321	0.563	0.681	0.751	0.796	0.827	0.851
0.05	−2.501	−0.431	0.163	0.425	0.568	0.657	0.784	0.816	0.852	0.876	0.894	0.907
0.1	−0.625	0.156	0.457	0.608	0.696	0.754	0.84	0.862	0.888	0.905	0.918	0.928
0.2	0.232	0.543	0.685	0.763	0.811	0.844	0.895	0.909	0.925	0.936	0.945	0.951
0.3	0.677	0.792	0.85	0.884	0.906	0.921	0.945	0.952	0.96	0.966	0.97	0.974
0.4	1.266	1.196	1.156	1.13	1.111	1.097	1.073	1.065	1.056	1.049	1.044	1.039
0.5	4.116	6.738	−21.923	−2.282	−0.684	−0.108	0.448	0.555	0.661	0.728	0.773	0.805

(*Table A1 Continued*)

a_p η\A	3	4	5	6	7	8	10	12	14	16	18	20
B												
0.6	−2.122	−0.33	0.21	0.453	0.588	0.672	0.792	0.823	0.857	0.88	0.897	0.91
0.7	−0.55	0.181	0.47	0.616	0.702	0.758	0.843	0.865	0.89	0.907	0.92	0.929
0.8	−0.159	0.349	0.565	0.68	0.749	0.795	0.865	0.883	0.904	0.919	0.93	0.938
0.9	0.027	0.436	0.618	0.716	0.776	0.816	0.878	0.894	0.913	0.926	0.936	0.944
1	0.139	0.491	0.652	0.739	0.793	0.83	0.886	0.902	0.919	0.931	0.941	0.948
E												
0.01	−7.662	9.893	2.668	1.493	1.024	0.775	0.517	0.387	0.308	0.256	0.219	0.191
0.05	3.124	1.402	0.872	0.625	0.484	0.394	0.286	0.224	0.184	0.156	0.135	0.12
0.1	1.455	0.83	0.567	0.427	0.341	0.284	0.211	0.168	0.14	0.119	0.104	0.092
0.2	0.684	0.447	0.328	0.258	0.212	0.179	0.137	0.111	0.093	0.08	0.07	0.063
0.3	0.28	0.199	0.153	0.124	0.104	0.09	0.07	0.058	0.049	0.042	0.037	0.034
0.4	−0.254	−0.203	−0.171	−0.147	−0.13	−0.116	−0.096	−0.081	−0.071	−0.063	−0.056	−0.051
0.5	−2.825	−5.697	24.143	3.602	1.906	1.284	0.77	0.547	0.423	0.344	0.29	0.251
0.6	2.793	1.307	0.825	0.595	0.463	0.378	0.276	0.216	0.178	0.151	0.131	0.116
0.7	1.374	0.798	0.55	0.416	0.333	0.277	0.207	0.165	0.137	0.117	0.102	0.091
0.8	1.019	0.631	0.448	0.345	0.28	0.235	0.177	0.142	0.118	0.102	0.089	0.079
0.9	0.85	0.543	0.392	0.305	0.249	0.21	0.159	0.128	0.107	0.092	0.081	0.072
1	0.748	0.488	0.356	0.279	0.228	0.193	0.147	0.119	0.1	0.086	0.075	0.067